HHS Public Access

Author manuscript

Nat Neurosci. Author manuscript; available in PMC 2013 August 01.

Published in final edited form as:

Nat Neurosci. 2013 February ; 16(2): 201–209. doi:10.1038/nn.3307.

Timothy Syndrome is associated with activity-dependent dendritic retraction in rodent and human neurons

Jocelyn F. Krey[1], **Sergiu P. Pasca**[1], **Aleksandr Shcheglovitov**[1], **Masayuki Yazawa**[1], **Rachel Schwemberger**[1], **Randall Rasmusson**[2], and **Ricardo E. Dolmetsch**[1]

[1]Department of Neurobiology, Stanford University School of Medicine

[2]Department of Physiology and Biophysics, State University of New York at Buffalo

Abstract

L-type voltage gated calcium channels (LTCs) play an important role in neuronal development by promoting dendritic growth and arborization[1–3]. A point mutation in $Ca_V1.2$ causes Timothy Syndrome (TS)[4], a neurodevelopmental disorder associated with autism spectrum disorders (ASD). We report that channels with the TS mutation cause activity-dependent dendrite retraction in rodent neurons and in induced pluripotent stem cell (iPSCs)– derived neurons from individuals with TS. Dendrite retraction is independent of calcium permeation through the mutant channel, is associated with ectopic activation of RhoA and is inhibited by over-expression of the channel associated GTPase Gem. These results suggest that $Ca_V1.2$ can activate RhoA signaling independently of Ca^{2+} and provide novel insights into the cellular basis of TS and other ASDs.

Voltage-gated calcium channels (VGCCs) such as $Ca_V1.2$ are essential for coupling electrical events to the activation of intracellular signaling pathways that control the development and function of neurons[5]. Mutations in VGCC genes have been linked to various neurological and psychiatric disorders, including epilepsy, ataxia, migraine, ASDs and schizophrenia[6–10]. While a great deal is understood about how disease-causing mutations change the biophysical properties of these channels[11,12], little is known about how these mutations alter neuronal development and cause disease. Elucidating this relationship is critical for understanding how mutations in VGCCs ultimately lead to neuronal dysfunction and regulate neuronal signaling under non-pathological conditions.

LTCs are characterized by their large single channel conductance, activation at depolarized potentials, and sensitivity to dihydropyridines[13]. The α1 subunit of the channel contains the

Corresponding Author: Ricardo E. Dolmetsch, PhD, Department of Neurobiology, Stanford School of Medicine, 299 Campus Drive D227, Stanford, California 94305, USA, ricardo.dolmetsch@stanford.edu, Tel.: 650-723-9812, Fax: 650-725-3958.

The authors have no competing financial interests.

AUTHOR CONTRIBUTIONS

R.E.D and J.F.K. designed the experiments and wrote the manuscript; J.F.K. performed all of the cellular assays in rodent cells, including the calcium imaging and immunocytochemistry studies, all of the mice breeding, and the *in vivo* studies of dendritic arborization; S.P.P differentiated the iPSC into neurons and performed the dendritic arborization experiments in human cells; A.S. performed and analyzed the electrophysiology; M.Y. generated and characterized the iPSCs; R.S. contributed to the analysis of dendrites in iPSC-derived neurons; R.R. generated the TS mice.

voltage sensor and ion pore, and forms a complex with β and α2δ subunits that regulate channel trafficking and gating[13,14]. $Ca_V1.2$ is the most abundant of the three LTCs in the mammalian brain and is expressed on the cell body, dendrites, and growth cones of developing neurons[15,16]. Timothy Syndrome (TS) is a multi-system disorder characterized by cardiac arrhythmias, webbing of the fingers and toes, hypoglycemia, and autism[4]. It is caused by a dominant mutation in an alternatively spliced exon of the *CACNA1C* gene, which encodes the α subunit of the L-type VGCC, $Ca_V1.2$[4]. The TS mutation is a glycine-for-arginine substitution at position 406 in the first of three intracellular loops in $Ca_V1.2$ that alters the ability of $Ca_V1.2$ to undergo voltage- and calcium-dependent inactivation. The TS mutation thus presents an excellent opportunity to examine the importance of these processes in neuronal development and function.

A major function of $Ca_V1.2$ is to regulate dendritic refinement in response to electrical activity[1–3]. Dendritic arbors are essential for information processing by neurons and play a key role in the formation of the neuronal circuits that underlie cognition[3]. Precisely how LTCs regulate dendritic development is not well understood. Although LTCs can activate transcription factors such as CREB and CREST that control the expression of genes involved in dendritic arborization[2,17], there is significant evidence that activity-dependent arborization also involves local activation of signaling pathways in dendrites[18–20]. The RGK (Rad, Rem, Rem2, Gem/Kir) family of small GTP binding proteins provides a potential link between $Ca_V1.2$ channels and dendritic arborization. Gem and Rem2 are both expressed in neurons[21,22] and bind to the β subunit of voltage-gated Ca^{2+} channels[23,24]. Although the function of RGKs in neurons is not well understood, they have been shown to regulate channel function both by altering channel trafficking[24–26] and by directly reducing channel activity[23,27]. The RGK proteins have also been reported to regulate signaling proteins that control dendritic arbors like Rho-GAP, Gem Interacting Protein (GMIP)[28], and the Rho kinase ROK1[29]. Whether the RGK proteins connect voltage-gated Ca^{2+} channels to the signaling pathways that regulate dendritic morphology is not known.

In this study, we used animal and human models of TS to study the effects of the TS mutation on dendritic arbors both *in vitro* and *in vivo*. *In vitro* we found that expression of $Ca_V1.2$ channels with the TS mutation triggers dendrite retraction when these neurons are stimulated electrically, either by bath depolarization or by activation of channelrhodopsin-2. *In vivo*, we observed changes in the dendritic arbor of neurons in a knock-in mouse model of TS. To show that the defects observed in rodents also occur in humans with TS, we generated iPSC-derived neurons from individuals with TS and proved that these cells also exhibit activity-dependent dendrite retraction. In studying the mechanism underlying these defects, we discovered that dendrite retraction triggered by the TS mutation is independent of Ca^{2+} flux through the channel. Instead, conformational changes in the $Ca_V1.2$ channel activate RhoA signaling via the small G protein Gem leading to dendrite retraction in response to electrical activity. These results identify a novel mechanism by which $Ca_V1.2$ can regulate signaling cascades in neurons and provide important insights into the pathophysiology of TS and other ASDs.

RESULTS

TS channels cause dendrite retraction in rat neurons

While voltage-gated calcium channels are known to play a key role in dendrite growth in many systems their importance in regulating dendrite development in cortical neurons has not been established. We first investigated which types of channels are important for controlling dendritic arbors in developing cortical neurons and found that blockers of LTCs completely eliminate dendrite growth in response to depolarization whereas other channel blockers have no significant effect (Supplementary Figs. 1 and 2a–d). To investigate the effects of the TS mutation on activity-dependent arborization, we introduced wild type (WT) or TS-$Ca_V1.2$ channels together with YFP into rat cortical neurons. We used anti-$Ca_V1.2$ antibodies to show that WT and TS $Ca_V1.2$ channels were expressed at levels similar to those of the endogenous channel, and that both channels were localized at the cell membrane (Supplementary Fig. 2e–f and Fig. 3). We then used fluorescence microscopy to measure changes in the dendritic arbor of individual cells over the course of nine hours. We observed no differences in the length of the dendritic arbors in resting neurons expressing TS or WT channel. However, activation of LTCs by depolarization caused a pronounced increase in the length and complexity of the dendritic arbor in neurons expressing WT channels (Fig. 1a–b). In contrast, depolarization caused a dramatic reduction in dendrite length in neurons containing TS-$Ca_V1.2$. This retraction was not due to an increase in apoptosis or necrosis, as we did not observe any differences in TUNEL staining or nuclear condensation between TS and control neurons (Supplementary Fig. 3).

Dendrite growth is the sum of dynamic extension and retraction events over the course of minutes and hours, and changes in either the number of extension or retraction events or in the amplitude of each event can lead to changes in the total dendrite length. To determine whether the TS channel affects either the number or length of dendritic retraction or extension events, we used high frequency time-lapse imaging to capture these events over the course of one hour. Dendrites from neurons expressing WT-$Ca_V1.2$ underwent slightly more extension than retraction events leading to a net growth of the dendritic arbor. In contrast, neurons expressing TS-$Ca_V1.2$ showed an increase in the number of dendritic retraction events and a decrease in the number of extension events, resulting in an overall decrease in dendrite length (Fig. 1c–d). There was no difference in the amplitude of individual retraction or extension events between cells expressing TS or WT channels (Supplementary Fig. 4), suggesting that activation of TS-$Ca_V1.2$ causes dendrite retraction by increasing the frequency of retraction events and not the amplitude of each event.

While membrane depolarization is a robust way of activating LTCs in culture, it is not a physiological stimulus for most neurons. To mimic physiological activation, we introduced channelrhodopsin-2 into rat neurons expressing TS or WT channels and electrically activated the cells by illuminating them with blue light. Patch clamp recordings showed that neurons fired high frequency bursts of action potentials for the duration of the illumination (Fig. 1e). We stimulated the cells to generate four one-second-long bursts of action potentials every thirty minutes over the course of twelve hours, and collected time-lapse images of the dendritic arbor every thirty minutes (Fig. 1f). Cells expressing the TS channel

showed a significant decrease in dendritic outgrowth when compared to cells expressing the WT channel (Fig. 1g), confirming that the TS channel causes dendrite retraction when neurons are stimulated with physiological patterns of electrical activity.

Brains from TS mice show defects in dendritic development

To study the consequences of the TS mutation on neuronal development *in vivo*, we generated a mouse model of TS[30]. Using homologous recombination, we introduced a cassette encoding the G406R point mutation that causes TS in humans into exon 8 of the mouse gene encoding $Ca_V1.2$. Mutations in the homologous exon in humans cause type-2 TS in patients. Breeding mice containing the TS mutation cassette produced only mice heterozygous for the *TS* allele, suggesting that the TS mutation is homozygous lethal in mice as it is in humans. There was no reduction in the size or viability of heterozygous $TS^{+/-}$ mice compared to WT littermates, and their gross brain size and structure appeared normal[30].

We compared the basal dendritic arbors of layer 2/3 pyramidal neurons from matched regions of the frontal cortex of WT and $TS^{+/-}$ littermates using Golgi staining. At postnatal day 7 (P7) we observed no significant difference in the total length or number of basal dendrites, suggesting that there are no gross defects in early dendritic development. By postnatal day 14 (P14), however, we observed a significant decrease in the total basal dendritic length and in the number of dendritic branches in neurons from $TS^{+/-}$ mice relative to WT littermates (Fig. 2a–f). In addition, the $TS^{+/-}$ mice had approximately six times more neurons with arbors smaller than 600 μM than WT littermates, and approximately one quarter as many neurons with arbors that exceed 1800 μM (Fig. 2h). The number of primary dendrites in neurons from $TS^{+/-}$ mice was also slightly decreased relative to controls, although this difference was not statistically significant (Fig. 2g). These findings suggest that the TS mutation has a dramatic effect on dendritic arborization at P14, and causes a net reduction in the basal dendritic complexity of cortical pyramidal neurons.

Human neurons from TS patients show dendrite retraction

Recent advances in somatic cell reprogramming[31] allow the study of human neurons differentiated *in vitro* from individuals with genetic neurodevelopmental diseases[32]. To determine whether the defects observed in rodents are also present in humans, we collected dermal fibroblasts from two TS patients and generated iPSC lines by infection with retroviruses containing SOX2, OCT3/4, Klf4 and c-Myc[33]. We differentiated the TS and control iPSC clones into cortical neurons using a four-stage protocol as previously described[34] (Fig. 3a). To measure dendrite development in human neurons, we infected the cells with an adeno-associated virus (AAV5) expressing YFP driven by the human synapsin-1 promoter. We then monitored changes in dendrite length in response to depolarization using time-lapse microscopy (Fig. 3b). Neurons derived from TS and control subjects showed similar changes in dendritic length at rest (the average change in total dendritic lengths during 30 min of incubation in a 5mM KCl solution was for TS: 3.67% ± 3.39 and for Ctrl: 5.62% ± 2.45; unpaired Student t-test, $p > 0.05$, mean ± s.e.m.), however depolarization led to a significant decrease in dendritic length in TS neurons while causing dendrite growth in control neurons (Fig. 3c–e). Depolarization caused an increase in the

number of retraction events and a decrease in the number of extension events (Fig. 3f), as observed in rat neurons (Supplementary Fig. 4b). These results suggest that human neurons derived from individuals with TS retract their dendrites in response to depolarization and therefore replicate the activity-dependent dendritic retraction observed in rat and mouse neurons carrying the TS mutation.

TS-dependent retraction is not due to excess Ca^{2+} influx

We next asked whether excess Ca^{2+} influx through the TS channels causes dendrite retraction. We measured calcium currents and calcium elevations in neurons expressing TS and WT channels. As previously reported[4,11,35], we found that the TS mutation decreased voltage dependent inactivation of the channel (Fig. 4a) and increased the Ca^{2+} rise triggered by depolarization of the neurons (Fig. 4b). To confirm that this increase depended on Ca^{2+} entering through TS-$Ca_V1.2$, we transfected neurons with WT or TS-$Ca_V1.2$ channels containing a 1036TY mutation (DHP- or TS-DHP), which renders the channels resistant to dihydropyridines such as nimodipine[36]. When these neurons were depolarized in the presence of nimodipine to block endogenous channels, cells expressing the TS-DHP had a substantially higher $[Ca^{2+}]_i$ rise than the WT DHP- channels (Supplementary Fig. 5) indicating that increased Ca^{2+} influx through the TS channel leads to an increase in $[Ca^{2+}]_i$ in neurons expressing these channels.

To determine whether the increased $[Ca^{2+}]_i$ caused by TS channels underlies activity-dependent dendritic retraction, we increased $[Ca^{2+}]_i$ in WT neurons to levels similar to those observed in TS neurons by depolarizing the cells in the presence of elevated extracellular Ca^{2+} (10 mM $[Ca^{2+}]_e$) or the $Ca_V1.2$ agonist BayK 8644 (5 μM) (Fig. 4c). While both manipulations increased $[Ca^{2+}]_i$ to levels similar to those of TS neurons, neither caused dendrite retraction (Fig. 4d) suggesting that in the absence of the TS channel, elevating global $[Ca^{2+}]_i$ is not sufficient to trigger dendrite retraction. To provide further evidence that dendritic retraction caused by TS channels is not purely a consequence of elevated $[Ca^{2+}]_i$, we reduced extracellular Ca^{2+} concentrations ($[Ca^{2+}]_e$) in neurons expressing TS channels and measured activity-dependent dendritic retraction. Reducing $[Ca^{2+}]_e$ to 0.2 mM brought the plateau of $[Ca^{2+}]_i$ in TS neurons to WT levels (2 mM $[Ca^{2+}]_e$; Fig. 4e) but did not prevent dendritic retraction following depolarization (Fig. 4f). In fact, dendritic retraction was observed in TS neurons even in the nominal absence of extracellular Ca^{2+} strongly suggesting that Ca^{2+} influx is not required for this process.

Because altering extracellular Ca^{2+} can affect neuronal signaling in unexpected ways, we tested whether Ca^{2+} influx was required for activity-dependent dendrite retraction in TS neurons using an independent method. We introduced three glutamate-to-glutamine mutations in the selectivity filter of TS-$Ca_V1.2$ that prevent calcium influx through the channel (TS-$Ca_V1.2$ 3EQ)[37,38] and expressed these channels in rat neurons. Whole cell patch clamping verified that these channels did not carry any inward calcium or barium currents in cells (Fig. 4g) or cause any measurable increase in $[Ca^{2+}]_i$ upon depolarization (Fig. 4h). Upon depolarization, however, these calcium impermeable TS channels still caused dendrite retraction (Fig. 4i–j). Dendrite retraction wasn't observed in WT channels containing the 3EQ mutations, indicating that increased retraction is not a consequence of

introducing non-conducting channels into cells. Similar results were observed using channels containing four glutamate-to-glutamine mutations in the selectivity filter (4EQ) (Supplementary Fig. 6). Together these results strongly indicate that the TS channel causes dendrite retraction independently of its capacity to carry calcium.

Gem is required for activity-dependent dendritic extension

One hypothesis to explain these findings is that voltage-dependent conformational changes in the TS channel activate signaling cascades that promote retraction of dendrites in TS neurons. To identify these pathways, we investigated channel-interacting proteins that could be linked to signaling cascades known to alter the cytoskeleton. The RGK proteins (Rad, Rem, Rem2, Gem/Kir) are small G proteins that can regulate RhoA signaling and bind to the β subunit of calcium channels[24–26,28,29]. The β subunit binds to a domain of the α_1 subunit that is immediately downstream of the TS mutation in $Ca_V1.2$. We therefore explored whether these proteins could be important for TS-dependent dendrite retraction. We first used RT-PCR to determine which RGK proteins are expressed in cortical neurons and found both Gem and Rem2 expressed in these cells (Supplementary Fig. 7a). We next investigated whether either Rem2 or Gem are necessary for activity-dependent dendritic arborization by using shRNAs to reduce the expression of each protein in developing neurons. We generated three shRNAs to Rem2 and Gem and verified by Western blotting that these shRNAs reduced the expression of Rem2 or Gem proteins (Supplementary Fig. 7b–e). Reducing Rem2 expression had no effect on activity-dependent dendritic growth (Fig. 5a) but reducing Gem expression prevented activity-dependent dendritic arborization in a manner that was consistent with the effectiveness of each shRNA (Fig. 5b–c). The inhibition of activity-dependent dendritic arborization by the Gem shRNA #2 was specific as expression of a mutant Gem that is resistant to the shRNA could reverse this effect (Fig. 5d–e). These results suggest that Gem is necessary for activity-dependent dendritic growth in cortical neurons.

We next asked whether Gem over-expression could prevent TS-$Ca_V1.2$-mediated dendrite retraction. We introduced a Gem expression plasmid into WT- or TS-$Ca_V1.2$-expressing neurons and measured dendritic arborization. We found that exogenous expression of Gem had no effect on dendritic arborization in WT neurons but completely prevented dendritic retraction in TS-$Ca_V1.2$ expressing neurons (Fig. 6a). Gem over-expression also prevented dendritic retraction triggered by the TS-$Ca_V1.2$ 4EQ channel, which contains pore mutations that prevent Ca^{2+} influx (Fig. 6b). This suggests that Gem's ability to rescue TS-$Ca_V1.2$ mediated dendritic retraction is independent of the effects of Gem on intracellular Ca^{2+} levels.

Over-expression of Gem has been found to inhibit RhoA signaling and induce neurite outgrowth in several cell lines[26,28,29]. To determine if Gem acts as a global inhibitor of RhoA in neurons or whether its activity is dependent on a direct interaction with $Ca_V1.2$, we generated Gem mutants that do not bind to the β subunit[25]. Gem mutants bearing either a R196A or V223A mutation were no longer able to co-immunoprecipitate with the β subunit (Fig. 6c) but preserved their ability to increase neurite extension in a neuroblastoma cell line suggesting that they can still inhibit RhoA (Supplementary Fig. 8). We expressed the R196A

or V223A mutants in TS-$Ca_V1.2$ expressing neurons and measured dendritic retraction upon depolarization. We found that over-expression of either Gem mutant was unable to prevent TS-$Ca_V1.2$ mediated dendritic retraction (Fig. 6d). This suggests that interaction between the β subunit and Gem is required for Gem to prevent the dendritic retraction caused by TS-$Ca_V1.2$.

Gem has also been shown to inhibit $Ca_V1.2$ activity by interfering with the trafficking of the channel to the cell membrane[24]. We therefore explored the hypothesis that Gem expression prevented retraction by reducing the membrane expression of the TS-$Ca_V1.2$ channel. We transfected neurons with either WT or TS YH-$Ca_V1.2$ channels bearing an extracellular HA epitope tag, and measured the amount of HA immunofluorescence in unpermeabilized cells. Over-expression of Gem had no effect on the cell surface localization of WT or TS YH-$Ca_V1.2$ channels relative to a CFP control, suggesting that Gem over-expression does not significantly alter $Ca_V1.2$ membrane localization in cortical neurons (Supplementary Fig. 9).

Because loss of Gem causes dendrite retraction in WT neurons and over-expression reverses TS-mediated retraction we explored the hypothesis that TS-$Ca_V1.2$ channels may be less effective than WT channels at binding Gem. We performed co-immunoprecipitation experiments in lysates from neuroblastoma cells over-expressing a YFP-tagged WT or TS-$Ca_V1.2$ α subunit, an HA-β subunit and Flag-Myc-Gem. Both WT and TS-$Ca_V1.2$ α subunits were able to co-immunoprecipitate with Flag-Myc Gem, however, Gem co-immunoprecipitated with about half the amount of TS-$Ca_V1.2$ than WT-$Ca_V1.2$ channels (Fig. 6d–e). These results suggest that the TS-$Ca_V1.2$ channel is less efficient at binding Gem compared to WT channels and support the hypothesis that TS-$Ca_V1.2$ channels cause dendrite retraction by failing to interact with Gem. Taken together these results provide strong evidence that the interaction of $Ca_V1.2$ with Gem is important for the ability of the channel to control activity-dependent dendritic arborization.

RhoA activation is necessary for TS-dependent retraction

A possible down stream target of TS-$Ca_V1.2$ channels is the GTPase RhoA which mediates dendrite retraction in many cell types and genetic systems[39–41]. We therefore investigated whether activation of TS-$Ca_V1.2$ channels activates RhoA in cortical neurons. We measured Ser19 phosphorylation of myosin light chain 2 (MLC2), a biochemical event that is downstream of RhoA activation[42]. Under control conditions, cells expressing WT or TS-$Ca_V1.2$ channels show low levels of phosphorylated MLC2. Following depolarization TS-$Ca_V1.2$ expressing neurons show significantly higher levels of phospho-MLC2 than WT cells (Fig. 7a–b). This indicates that activation of the TS-$Ca_V1.2$ channel leads to upregulation of RhoA signaling. To determine if TS-$Ca_V1.2$ activation depends on Ca^{2+} influx, we investigated whether the TS-$Ca_V1.2$ 3EQ channel could increase phospho-MLC2 levels following depolarization. We found that TS-$Ca_V1.2$ increased significantly the levels of phospho-MLC2 levels (Fig. 7c) indicating that activation of RhoA is independent of Ca^{2+}.

We next investigated whether activation of RhoA in WT neurons can phenocopy the effects of the TS-$Ca_V1.2$ channel. We found that expression of a constitutively active form of RhoA (RhoV14) is sufficient to cause dendritic retraction (Fig. 7d). To determine whether

activation of RhoA is necessary to cause dendrite retraction in TS-$Ca_V1.2$ expressing neurons, we inhibited RhoA activation either by expression of a dominant negative form of RhoA (RhoN19; Fig. 7e) or application of a cell-permeable RhoA inhibitor (C3 transferase; Fig. 7f). Both RhoN19 expression and treatment with C3 transferase prevented activity-dependent retraction, suggesting that this pathway is required for the effects of the channel. Finally, we investigated whether exogenous expression of Gem prevents RhoA activation in TS neurons (Fig. 7g). We expressed Gem in neurons containing the TS channel and found significantly decreased levels of phospho-MLC2 in these cells suggesting that Gem prevents ectopic activation of RhoA by TS-$Ca_V1.2$. Taken together, these studies support a model by which a conformational change in the TS-$Ca_V1.2$ reduces recruitment of Gem leading to ectopic activation of RhoA. RhoA in turn activates a series of biochemical cascades that result in dendrite pruning and retraction.

DISCUSSION

The mutation that causes TS leads to decreased calcium- and voltage-dependent inactivation of the $Ca_V1.2$ channel, but the cellular consequences of this defect are not well understood. In this paper, we show that TS-$Ca_V1.2$ channels cause activity-dependent dendrite retraction in rat, mouse and human neurons. This retraction does not depend on excessive Ca^{2+} influx through the TS channel, but is mediated by a Ca^{2+}-independent mechanism. Our studies are consistent with a model in which activated $Ca_V1.2$ channels recruit Gem and thereby prevent activation of RhoA allowing dendrite retraction. The TS mutation prevents $Ca_V1.2$ from recruiting adequate levels of Gem, leading to ectopic activation of RhoA and dendrite retraction.

These studies provide novel insights into the pathophysiology of TS and other ASDs. Studies of brains from individuals with ASDs and ID suggest that impaired dendrite formation is a common feature of many neurodevelopmental disorders. Impaired mini-column formation has been observed in post-mortem brains from patients with ASDs[43], and it has been suggested that individuals with autism have changes in long-range and short-range neural connections[44,45]. Furthermore, a number of studies have identified defects in dendritic arborization in mouse models of disorders such as Rett syndrome and Fragile X[46,47]. Our data uncover a direct cellular link between the TS mutation in LTCs and defects in dendritic remodeling, and could shed light on the role of arborization defects in other developmental disorders.

In this paper we also show that activity-dependent dendritic retraction is observed in human neurons derived from individuals with TS. Although many studies in rodent models of ASD have been informative, there are examples where defects in animal models could not be confirmed in humans. Our study shows that dendrite retraction occurs in rodent neurons and in human neurons. This provides strong evidence that dendrite retraction is a feature of TS and shows that iPSC-derived neurons can recapitulate defects observed in neurons *in vivo*.

Our study also provides tantalizing new information about the mechanism by which the TS channel causes dendrite retraction. We found that dendritic retraction is independent of the amount of Ca^{2+} flux through the channel. This result is unexpected because changes in

$[Ca^{2+}]_i$ are thought to be central to LTC-mediated signal transduction in neurons. We have three lines of evidence that support this conclusion. First, elevating $[Ca^{2+}]_i$ in WT neurons to the same levels observed in TS neurons does not trigger dendrite retraction. Second, reducing extracellular Ca^{2+} in TS neurons, even to resting levels, does not prevent activity dependent retraction. Finally, introducing point mutations in the TS channel that prevent Ca^{2+} flux through the channel does not prevent the channel from triggering retraction. These results are consistent with the idea that $Ca_V1.2$ channels can activate signaling cascades by voltage-dependent conformational changes[48,49], reminiscent of the physical mechanism by which a related channel $Ca_V1.1$ causes excitation-contraction coupling in skeletal muscle[50].

A possible link between conformational changes in $Ca_V1.2$ and activation of RhoA is the RGK protein Gem. Gem directly binds to both the α and β subunits of $Ca_V1.2$ channels and can modulate channel gating. We found that Gem overexpression prevents dendritic retraction triggered by TS channels and this effect depends on the ability of Gem to bind to the channel. Interestingly, Gem is also required for dendritic arborization in control cells as reduction of Gem with shRNAs prevents activity dependent dendrite growth. The mechanism by which Gem controls dendrite growth in response to LTCs activation is unclear. One possibility is that activated $Ca_V1.2$ recruits Gem, which in turn causes local inhibition of RhoA preventing dendrite retraction and allowing dendrite extension. Gem and the other RGK proteins inhibit RhoA signaling by activating RhoA GAPs and by inhibiting the downstream kinase ROCK. By binding weakly to Gem, the TS channel fails to suppress RhoA activation and leads to dendrite retraction, which dominates over dendrite extension.

An alternative possibility is that Gem prevents retraction by forcing TS channels into an inactivated state where they no longer activate RhoA. This is consistent with the finding that Gem overexpression decreases LTC activity and Ca^{2+} influx in neurons by increasing the fraction of $Ca_V1.2$ channels in a non-conducting state. Interestingly, despite its negative effects on Ca^{2+} influx, Gem expression is required for activity-dependent dendritic arborization and Gem overexpression does not inhibit dendrite growth. This suggests that Gem is necessary for activating the signaling cascades that promote dendrite extension despite reduced Ca^{2+} influx across the membrane.

In summary, our studies show that the TS channel causes dendrite retraction in rodent and human neurons and identifies a novel signaling modality for the $Ca_V1.2$ channel. This sets the stage for further studies aimed at understanding the underlying mechanism of ASD and ID in these children. In addition, these results unveil a novel mode of signaling for LTCs that is independent of Ca^{2+} and directly links $Ca_V1.2$ channels to the regulation of RhoA signaling in the brain.

METHODS

DNA constructs

$Ca_V1.2$ Constructs—Construction of the wild-type (WT) and dihydropyridine-resistant $Ca_V1.2$ (DHP−) in the pcDNA4/HisMax vector has been previously described[36]. We generated plasmids encoding $Ca_V1.2$ N-terminally tagged with Flag/Myc epitopes as described previously using Gateway technology[51,52]. We generated YH- $Ca_V1.2$ plasmids

encoding $Ca_V1.2$ N-terminally tagged with YFP and containing an extracellular HA epitope tag in the S5-H5 loop of domain II as described previously[51]. Site-directed mutagenesis was performed with the QuickChange II XL kit (Stratagene) to generate the TS, WT 3EQ, TS 3EQ, and TS 4EQ mutant plasmids. The changed nucleotides are as follows: TS (G1216A), 3EQ (G1087C, G2116C, G3352C), 4EQ (G1087C, G2116C, G3352C, G4255C). Mutagenesis was always followed by full sequencing of the resulting channel. Primers and sequences are available upon request.

RhoA Constructs—pcDNA3 Flag-RhoA V14A and pcDNA3 Flag-RhoA N19A were a generous gift from Yukiko Gotoh. The sequences containing RhoA V14 and RhoA N19 were cut using BamHI and inserted into the pcDNA3 CFP- vector to generate either constitutively active RhoA (V14) or dominant-negative (N19) RhoA N-terminally tagged with CFP, which were then expressed in neurons. The pcDNA3 CFP- vector was used as a control.

RGK Constructs—The rat sequence of Gem (NM_001106637) or Rem2 (NM_022685) were cloned from cDNA prepared from mRNA isolated from rat embryonic day 18 (E18) cortex using the RNA Easy Kit (Qiagen). Plasmids encoding Myc-Gem or Myc-Rem2 were generated using Gateway technology (Invitrogen) by inserting the cloned rat Gem or Rem2 sequences into the TOPO sites of the pCR8 entry vector and then transferring the Gem or Rem2 coding sequence into the destination vector pDEST Flag/Myc-, which contains a CMV promoter and N-terminal Flag and Myc eptiope tags in frame with ATTR acceptor sequences. A pDEST Flag-Myc CFP plasmid was generated in the same fashion (except CFP was cloned from the pcDNA3 CFP-plasmid) and was used as a control in all experiments using the pDEST Flag-Myc Gem or Rem2 plasmids. Site-directed mutagenesis was performed with the QuickChange II XL kit (Stratagene) to generate plasmids encoding the Gem R196A and Gem V223A mutants described by Beguin and colleagues[25]. The following nucleotides were changed in the Gem coding sequence of the pDest Flag/Myc Gem construct: Gem R196A (C586G, G587C), Gem V223A (T668C). All constructs and mutations were verified by full sequencing of the plasmids. All primers and sequences are available upon request.

RGK shRNA constructs—Two 19-mer oligonucleotide sequences targeted against the rat Gem sequence were designed using the Whitehead Institute Bioinformatics and Research Computing siRNA design tool (http://jura.wi.mit.edu/bioc/siRNAext/). Two 19-mer oligonucleotide sequences targeted against the rat Rem2 sequence were based on shRNA sequences that have been previously published[53]. The oligonucleotide sequences are as follows: Gem shRNA#1 (GATACATATGAGCGTACCC), Gem shRNA#2 (CCATTATCCTACTGGACAT), Rem2 shRNA#1(GAACTCAGAGGACACCTAT), Rem2 shRNA#2(GACGGATCATGGTGGACAA). Short hairpin oligonucleotides were designed (using Clontech's shRNA sequence designer) and inserted into RNAi-Ready pSIREN-DNR-DsRed-Express vector (Clontech) by ligation into the BamHI and EcoRI sites. For the control shRNA, a luciferase shRNA annealed oligonucleotide (Clontech, provided with pSIREN vector) was annealed into the pSIREN-DNR-DsRed-Express vector following the same procedure. To generate a plasmid encoding a Gem protein resistant to suppression by

Gem shRNA #2, mutagenesis was performed as above on the pDEST Flag/Myc Gem construct. The three silent mutations were introduced into the Gem coding sequence with the following nucleotide changes: A384T, G387A, C390T. Mutations were verified by full sequencing and primers and sequences are available upon request.

Co-immunoprecipitation and Western blotting

To test effectiveness of shRNAs, HEK 293T cells grown in DMEM with 5% fetal bovine serum (FBS) were plated in 6-well plates and transfected by standard Ca^{2+} phosphate procedures[36]. Each well of the 6-well plate was transfected with 2 μg shRNA, 100 ng pDEST Flag-Myc Gem, Flag-Myc Gem-R, or Flag-Myc Rem2, and 100 ng of pDEST Flag-Myc CFP. Cells were lysed 36–48 hours post-transfection and immunoblots were prepared as described previously[52]. Briefly, cells were lysed in 1X SDS Buffer, lysates were boiled for 10 minutes at 100°C, and 10 μl of lysates were run on a 10% polyacrylamide gel. Membranes were blotted with an anti-Myc antibody (1:1000, 4-A6, Upstate Biotechnology). ImageJ (NIH) was used to quantify the intensity of the bands. The intensity of the RGK (Gem, Gem-R, or Rem2) band was normalized to the intensity of the Myc-CFP band in the same lane, which was used as a transfection and loading control.

The Gem/β3 co-immunoprecipitation experiments were performed using HEK 293T cells grown in DMEM with 5% FBS and transfected by standard Ca^{2+} phosphate procedures[36]. Each well of the 6-well plate was transfected with 1 μg pDEST Flag-Myc Gem, 1 μg HA-β3, or 1 μg of each alone. Cells were lysed 18–24 hours post-transfection with 300 μl lysis buffer (50 mM Tris pH 7.5, 100 mM NaCl, 1 mM MgCl2, 0.5% Triton X-100) per well. Protease inhibitor cocktail tablets (Roche Diagnostics) were added to lysis buffer immediately before lysing cells. Cell lysates were incubated for 1 hour at 4°C, centrifuged for 15 minutes to remove cell debris, and 250 μl of supernatant was incubated with 25 μl of anti-Flag M2 agarose beads (Sigma) for 3–4 hours at 4°C. Agarose beads were rinsed three times for 15 minutes each in lysis buffer, and then proteins were eluted with 50 μl of 1X SDS buffer, boiled for 8 minutes at 95°C and frozen at −80°C. Elutions were run on 10% polyacrylamide gels using standard western blot protocols and membranes were blotted with either anti-Myc antibody (1:1000, 4A6, Upstate Biotechnology) or anti-HA 3F10 antibody (1:1000, Roche).

The YFP-$Ca_V1.2$/Gem/β3 co-immunoprecipitation experiments were performed using Neuro2a cells grown in MEME with 10% FBS in 10cm dishes and transfected using Lipofectamine 2000 (Invitrogen) following manufactur's instructions. Each 10cm plate was transfected with 6 μg pDEST Flag-Myc Gem, 6 μg HA-β3, and/or 12 μg of YFP-Cav1.2. Cells were lysed 22–24 hours post-transfection with 1 ml lysis buffer (50 mM Tris pH 7.5, 100 mM NaCl, 1 mM MgCl2, 1% Triton X-100) per plate. Protease inhibitor cocktail tablets (Roche Diagnostics) were added to lysis buffer immediately before lysing cells. Cells lysates were incubated for 1 hour at 4°C, centrifuged for 15 minutes to remove cell debris, and 900 μl of supernatant was incubated with 40 μl of anti-Flag M2 agarose beads (Sigma) for 3–4 hours at 4°C. Agarose beads were rinsed two times for 15 minutes each in lysis buffer, then one time for 15 minutes in 1× TBS and then proteins were eluted with 150 ng/μl 3X Flag peptide for 30 minutes at 4°C. Supernatant was then mixed with 2× SDS sample buffer and

boiled for 5 minutes at 85°C. Elutions (10μl of each) were run on 4–12% Bis-Tris gradient gels using standard western blot protocols and membranes were blotted with either anti-GFP rabbit serum (1:1000, Invitrogen Molecular Probes), anti-Myc antibody (1:1000, 4A6, Upstate Biotechnology) or anti-HA 3F10 antibody (1:1000, Roche).

Dissociated Cell Cultures and Transfections

Cortical neurons from E17–E19 Sprague Dawley rats (*Rattus Norvegicus*) were cultured as described previously[54] and plated at 1×10^6 neurons/ml on poly-ornithine- and laminin-coated 24- or 96-well tissue culture plates. Neurons were maintained in Basal Medium Eagle with 5% FBS, 100 units/mL Penicllin, 100 μg/mL Streptomycin, 2 mM L-glutamine and 1% glucose. Neurons were transfected using Lipofectamine 2000 (Invitrogen) and assayed 30–48 hours following transfection. For the dendritic arborization assay, Ca^{2+} imaging and phospho-MLC2 assay, neurons were transfected at 2–3 days in vitro (DIV) with a 2:2:0.5 ratio of α1c (pcDNA4 $Ca_V1.2$), β1b, and YFP constructs. Molar ratios have been optimized so that the majority (>70%) of YFP-positive neurons also express the exogenous channel. For dendritic arborization assays using shRNAs targeting Gem, neurons were transfected at 2–3 DIV with a 2:0.5 ratio of pSIREN shRNA and pGW1 YFP, and imaged 48–72 hours after transfection. The DsRed expression from the pSIREN construct was used to determine co-transfection efficiencies and >90% of cells expressing YFP also expressed the shRNA. For dendritic arborization assays involving RhoV14 or RhoN19 expression neurons were transfected with a 1:0.5 ratio of pcDNA3 CFP-RhoV14 (or pcDNA3 CFP-as control) and pGW1 YFP plasmids or with a 2:2:1:0.5 ratio of α1c (pcDNA4 CaV1.2): β1b: pcDNA3 CFP-RhoN19: YFP constructs. The same ratios were used for dendritic arborization assays involving Gem overexpression with pDest Flag/Myc CFP (control) or pDEST Flag/Myc Gem replacing the RhoN19 construct. For all experiments ratios were optimized so that the majority (>70%) of YFP-positive neurons also co-expressed the channel and other co-transfected proteins.

Dissociated Culture Immunocytochemistry

Dissociated cortical neurons were plated at 5×10^5 neurons/well on 15 mm coverslips placed in 24-well tissue culture plates. Thirty-six to forty-eight hours following transfection, neurons were fixed in 4% paraformaldehyde/2% sucrose, permeabilized with 0.25% Triton X-100 and blocked in 3% bovine serum albumin (BSA) in phosphate-buffered saline (PBS). Neurons were incubated with anti-Myc antibodies (1:1000, 4A6, Upstate Biotechnology) or anti-$Ca_V1.2$ antibodies (1:150, Chemicon AB5156) diluted in 3% BSA followed by incubation with Alexa594 conjugated secondary antibodies (1:1000, Invitrogen) and then counterstained with Hoechst 33258 (Molecular Probes, 1:10,000) for 15 minutes prior to mounting. YH-$Ca_V1.2$ expressing neurons were stained as outlined previously[51]. Briefly, neurons were fixed with 4% paraformaldehyde, blocked with 3% BSA, incubated with an anti-HA 3F10 antibody (1:1000, Roche Cat. Na. 12158167001) and treated with a goat anti-rat Alexa 594 secondary antibody (1:1000, Molecular Probes). Slides were visualized by epifluorescence microscopy using a cooled CCD camera (Hamamatsu) coupled to an inverted Nikon Eclipse E2000-U microscope and OpenLab 4 software (Improvision).

Phospho-MLC2 Assays

Twenty-four to thirty-six hours following transfection, neurons were placed in a control Tyrode's solution or depolarized in a 65 mM KCl Tyrode's solution for 1 hour and then fixed with 4% paraformaldehyde in PBS for 10–15 minutes at room temperature. Neurons were then washed with 1X PBS two times and blocked in 3% BSA + 0.25% Triton X-100 in PBS for 30 minutes at room temperature. Neurons were then incubated with anti-phospho-myosin light chain 2 (Ser19) antibodies (1:1000, Cell Signaling Technology) diluted in 3% BSA overnight at 4°C. Neurons were then incubated with Alexa594 conjugated secondary antibodies (1:1000, Invitrogen) for 1 hour and then counterstained with Hoescht 33258 (1:10,000) for 10 minutes prior to mounting coverslips on slides. Slides were visualized by epifluorescence microscopy using a cooled CCD camera (Hamamatsu) coupled to an inverted Nikon Eclipse E2000-U microscope and OpenLab 4 software (Improvision). The fluorescence intensity of phospho-MLC2 staining in YFP-positive neurons was quantified using OpenLab 4 software. At least 50 cells were quantified in each condition, and experiments were repeated at least 3 times. A histogram of intensity values in the control or stimulated conditions was used to determine a threshold value that separated pMLC2-positive cells from background staining. This value was used to quantify the percentage of cells in each condition that were pMLC2-positive.

Ca^{2+} Imaging

Cortical neurons were loaded with 1 mM Fura-2 acetoxymethyl ester (Invitrogen) for 30 minutes at 37°C in cortical medium and placed in a specialized imaging chamber. Neurons were pre-incubated and imaged in Tyrode's solution (129 mM NaCl, 5 mM KCl, 2 mM $CaCl_2$, 1 mM $MgCl_2$, 30 mM glucose, 25 mM Hepes, 0.1% BSA) for 100 ms followed by perfusion with a Tyrode's solution containing elevated potassium (75 mM NaCl, 67 mM KCl, 2 mM $CaCl_2$, 1 mM $MgCl_2$, 30 mM glucose, 25 mM Hepes, 0.1% BSA). Imaging of selected transfected neurons (YFP-positive) was performed at 25°C on an inverted epifluorescence microscope with cooled CCD camera and automated stage. Time-lapse excitation-ratio images were collected and quantified using OpenLab 4 software as described previously[36]. Values were converted to $[Ca^{2+}]_i$ using standard calibration procedures.

Electrophysiology

HEK-293 cells were grown in EMEM (30–2003, ATCC) supplemented with 10% FBS, penicillin G (100 U/ml), and streptomycin (0.1 mg/ml). Cells plated in 35 mm dishes were transiently transfected with pcDNA4 $Ca_V1.2$ plasmids containing WT or mutant $Ca_V1.2$ (2μg), β1b (0.7μg), α2δ (0.7μg), T-antigen (0.5μg) and YFP (0.1μg), using JET-PEI (Qbiogene, Montreal, Canada). YFP-positive cells were recorded 36–48 hours after transfection. Whole cell currents were recorded using a EPC 10 amplifier (HEKA) in the following external solution (in mM): 5 BaCl2, 170 TEACl, and 10 HEPES, pH adjusted to 7.4 with TEAOH. Pipette solution contained (in mM): 122 Cs-Asp, 10 EGTA, 5 MgCl2, 4 Mg-ATP, 0.4 Na-GTP, and 10 HEPES, pH adjusted to 7.4 with CsOH. Data was filtered at 2 kHz and digitized at 5 kHz. Neuronal responses to the light stimulation were measured in current clamp mode using the following extracellular and intracellular solutions (in mM):

129 NaCl, 5 KCl, 2 CaCl2, 1 MgCl2, 30 Glucose, 25 HEPES, pH 7.4 – extracellular; 120 KGlu, 20 KCl, 4 NaCl, 4 Mg2ATP, 0.3 NaGTP, 10 Na2PCr, 0.5 EGTA, 10 HEPES, pH 7.25 – intracellular. Data was filtered and digitized as above.

Photostimulation

For experiments using light to stimulate cells electrically, dissociated hippocampal neurons were first infected with viruses carrying channelrhodopsin-2 (ChR2). Rat hippocampal neurons were obtained from E18 embryos as described elsewhere[55]. Cells were plated on polyornithine/laminin-coated coverslips at low density (10^5 cells per well in 24 well-plates) and cultured in Neurobasal media supplemented with B27 and L-glutamine (all from Invitrogen). To produce viruses, 90% confluent HEK 293T cells (ATCC) cultured in 10cm dishes were transfected with pLenti-CaMKII-hChR2 (H134R)-EYFP-WPRE[56] (Addgene plasmid 20944; (10 μg), VSVG (5 μg) and d8.2 (10 μg) using Lipofectamine 2000 reagent (Invitrogen) (30 μl). After 15–20 hours, media was changed to neuronal culturing media, in which cells were kept for an additional 20–24 hours. This conditioning media containing viral particles was filtered and immediately used for neuronal transduction.

To perform photostimulation experiments, dissociated hippocampal neurons were initially cultured for 6 – 7 hours in the conditioning media containing viral particles. Under these experimental conditions, ~ 80 – 90% of neurons were fluorescent after four days in culture (DIC). At 3 – 4 DIC, neurons were transfected with plasmids containing CaV1.2- or CaV1.2-TS, and YFP at a 1:1:0.1 ratio using Lipofectamine 2000 reagent (Invitrogen). We optimized the number of days in culture, light intensity and the duration of light exposure to achieve reliable induction of action potentials in ChR2-expressing neurons without compromising survival. Photostimulation experiments were carried out 6 days after transfection (9 DIC) using a Zeiss Observer.Z1 microscope (Carl Zeiss) equipped with automated stage, X-Cite light source (EXFO), and 10X objective. During each experiment, neurons were kept in modified Tyrode's solution (129mM NaCl, 5mM KCl, 2mM CaCl2, 1mM MgCl2, 30mM Glucose, 25mM HEPES, pH 7.4) supplemented with 2% B27 at 32–34°C. All imaging experiments were performed using the Volocity software (Improvision Inc). For image analysis, background correction was performed in Adobe Photoshop SC3 using the Levels function so that the brightest and the darkest pixels had the same intensity in all the pictures.

To analyze dendritic arborizations in these experiments, we used the HCA-vision software (CSIRO), which performs a semi-automatic analysis of cell morphology. Parameters for dendrite detection, once set, were kept constant for all the pictures. Statistical analysis was done using Excel (Microsoft) and Prism 5 (GraphPad).

Dendritic Arborization Assay and Time-lapse Imaging

Thirty-six to forty-eight hours following transfection, neurons were placed in a control Tyrode's solution or stimulated with Tyrode's solution containing 67 mM KCl and time-lapse images of cells were taken over a 9-hour stimulation period at 10× magnification, using a high-throughput automated epi-fluorescence microscope with an environmentally controlled stage (ImageXpress, Molecular Devices). Imaging was performed on duplicate

wells, with at least 20 images taken per well. Individual YFP-positive neurons were chosen in a blinded fashion such that the researcher was unaware of the treatment condition (well numbers were randomly recoded using an automated computer program). For each cell, dendrites were traced and measured at the 0 and 9 hour time points using ImageJ and NeuronJ programs[57]. The change in the number and length of primary dendrites and branch dendrites for each neuron was then measured and calculated. Similar methods were also used to perform time-lapse imaging analysis of neurons placed in a control Tyrode's solution or stimulated with Tyrode's solution containing 67 mM KCl, and imaged every 10 minutes over a 60 to 80 minute period.

Golgi staining of mouse brain and analysis of layer 2/3 dendritic arbors

TS$^{+/-}$ mice (*Mus Musculus*) containing the G406R mutation in exon8A of the *CACNA1C* gene were generated as described previously[30]. Mice were backcrossed onto a C57BL/6J background and both male and female mice were used for all analyses. Golgi staining on brains from postnatal day 7 or 14 WT and *TS*$^{+/-}$ littermate mice was performed using the Rapid GolgiStain Kit (FD Neurotechnologies) following the manufacturers instructions. Briefly, brains from postnatal day 14 mice were removed and immersed in Golgi solution (solution A + solution B) in the dark for 2 weeks. Brains were then cryoprotected for at least 48 hours in solution C, sectioned at 150 μm thickness on a microtome, mounted onto gelatin-coated slides, and developed following the manufacturer's protocol. Matched sections containing the frontal cortex were imaged using a 20X objective and brightfield illumination on a Zeiss Axioimager M1 microscope with HRM digital camera system. Z-stacks were collected at 20× across the width of the section and exported to Neurolucida software (MBF Biosciences) for analysis. The basal dendritic arbors of cortical layer 2/3 pyramidal neurons were reconstructed and measured using Neurolucida. All imaging and anaylsis was done blinded to the genotype of the mice. All experiments on mice or rats were performed in accordance with protocols approved by the Institutional Animal Care and Use Committee (IACUC) at Stanford University and following NIH guidelines for animal welfare.

iPSC generation and neural differentiation

The iPSC clones were generated using retroviruses from fibroblasts harvested from two individuals with TS and two healthy subjects, as previously reported[33,34]. Informed written consent was obtained from all human subjects used for this study. Two lines (clones) from one TS patient (T7643-7 and T7643-32), one line from a second TS patient (T9862-61) and three lines from two unaffected controls (NH2-6, IM23-16, IM23-9) were differentiated into neurons and used for live imaging dendrite tracing. All the iPSC lines used in this study were extensively characterized previously[33,34]. Neural differentiation of the pluripotent stem cells was performed as previously described[34]. Briefly, cellular aggregates were generated from iPSC colonies by enzymatic dissociation and kept in suspension for five days. For neural induction, the cellular aggregates were plated on a polyornithine/laminin-rich substrate. After ten days, neural rosettes were mechanically isolated and expanded in suspension as neurospheres for an additional seven days prior to the initiation of differentiation by replating, FGF2/EGF withdrawal and the addition of BDNF and NT3. The

vast majority of neurons obtained with this protocol expressed cortical layer specific markers, as assessed by single cell qPCR[34].

Tracing of dendrites in iPSC-derived neurons

Neuronal cultures, after 5 weeks of *in vitro* differentiation were infected with an adeno-associated virus (AAV5) carrying a YFP reporter gene under the control of the human Synapsin-1 promoter. Neurons expressing YFP under this promoter were imaged after 50–70 days of *in vitro* differentiation. For live imaging, neurons were grown on 15 mm glass coverslips (Warner Instruments) and placed in a perfusion chamber on the stage of confocal microscope (PerkinElmer) in a 5mM KCl Tyrode solution containing 2% B27 (Invitrogen). After 30 minutes of imaging in a 5mM KCl solution, a 67mM KCl solution containing 2% B27 was injected in the chamber. Experiments were performed at ~30°C. Total dendrite length of individual Synapsin-1 expressing neuron, before and after 2 hours of depolarization, was traced semi-automatically using the HCA-Vision software (CSIRO, Australia). For assessing the number of retraction and extension events, cells were imaged every 5 minutes with a 40× objective (Fig. 3d, 3f).

Supplementary Material

Refer to Web version on PubMed Central for supplementary material.

ACKNOWLEDGMENTS

We thank Katharine Timothy and the TS patients who participated in this study, John Bernstein and Joachim Hallmayer for recruiting the subjects for this study, and Elizabeth Nigh for critical reading of the manuscript. J.F.K. was supported by a National Research Service Award (NRSA) predoctoral fellowship. Financial support was provided by an NIH Director's Pioneer Award and a Simons Foundation Grant to R.E.D., the International Brain Research Organization (IBRO) Outstanding Research Fellowship and the Tashia and John Morgridge Endowed Fellowship to S.P.P., a Japan Society of the Promotion for Science Postdoctoral Fellowship for Research Abroad and American Heart Association Western States to M.Y., a CIRM Postdoctoral Fellowship to O.S. We are also grateful for funding from B. and F. Horowitz, M. McCafferey, B. and J. Packard, P. Kwan and K. Wang.

REFERENCES

1. McAllister AK, Katz LC, Lo DC. Neurotrophin regulation of cortical dendritic growth requires activity. Neuron. 1996; 17:1057–1064. [PubMed: 8982155]
2. Redmond L, Kashani AH, Ghosh A. Calcium regulation of dendritic growth via CaM kinase IV and CREB-mediated transcription. Neuron. 2002; 34:999–1010. [PubMed: 12086646]
3. Wong RO, Ghosh A. Activity-dependent regulation of dendritic growth and patterning. Nat Rev Neurosci. 2002; 3:803–812. [PubMed: 12360324]
4. Splawski I, et al. Ca(V)1.2 calcium channel dysfunction causes a multisystem disorder including arrhythmia and autism. Cell. 2004; 119:19–31. [PubMed: 15454078]
5. Dolmetsch R. Excitation-transcription coupling: signaling by ion channels to the nucleus. Sci STKE. 2003; 2003:PE4. [PubMed: 12538881]
6. Tonelli A, et al. Early onset, non fluctuating spinocerebellar ataxia and a novel missense mutation in CACNA1A gene. J Neurol Sci. 2006; 241:13–17. [PubMed: 16325861]
7. Wang K, et al. Common genetic variants on 5p14.1 associate with autism spectrum disorders. Nature. 2009; 459:528–533. [PubMed: 19404256]
8. Nyegaard M, et al. CACNA1C (rs1006737) is associated with schizophrenia. Mol Psychiatry. 2010; 15:119–121. [PubMed: 20098439]

9. Tottene A, et al. Familial hemiplegic migraine mutations increase Ca(2+) influx through single human CaV2.1 channels and decrease maximal CaV2.1 current density in neurons. Proc Natl Acad Sci U S A. 2002; 99:13284–13289. [PubMed: 12235360]
10. Splawski I, et al. CACNA1H mutations in autism spectrum disorders. J Biol Chem. 2006; 281:22085–22091. [PubMed: 16754686]
11. Barrett CF, Tsien RW. The Timothy syndrome mutation differentially affects voltage- and calcium-dependent inactivation of CaV1.2 L-type calcium channels. Proc Natl Acad Sci U S A. 2008; 105:2157–2162. [PubMed: 18250309]
12. Hoda JC, Zaghetto F, Singh A, Koschak A, Striessnig J. Effects of congenital stationary night blindness type 2 mutations R508Q and L1364H on Cav1.4 L-type Ca2+ channel function and expression. J Neurochem. 2006; 96:1648–1658. [PubMed: 16476079]
13. Catterall WA. Structure and regulation of voltage-gated Ca2+ channels. Annu Rev Cell Dev Biol. 2000; 16:521–555. [PubMed: 11031246]
14. Richards MW, Butcher AJ, Dolphin AC. Ca2+ channel beta-subunits: structural insights AID our understanding. Trends Pharmacol Sci. 2004; 25:626–632. [PubMed: 15530640]
15. Pravettoni E, et al. Different localizations and functions of L-type and N-type calcium channels during development of hippocampal neurons. Dev Biol. 2000; 227:581–594. [PubMed: 11071776]
16. Hell JW, et al. Identification and differential subcellular localization of the neuronal class C and class D L-type calcium channel alpha 1 subunits. J Cell Biol. 1993; 123:949–962. [PubMed: 8227151]
17. Aizawa H, et al. Dendrite development regulated by CREST, a calcium-regulated transcriptional activator. Science. 2004; 303:197–202. [PubMed: 14716005]
18. Lohmann C, Wong RO. Regulation of dendritic growth and plasticity by local and global calcium dynamics. Cell Calcium. 2005; 37:403–409. [PubMed: 15820387]
19. Fink CC, et al. Selective regulation of neurite extension and synapse formation by the beta but not the alpha isoform of CaMKII. Neuron. 2003; 39:283–297. [PubMed: 12873385]
20. Lohmann C, Myhr KL, Wong RO. Transmitter-evoked local calcium release stabilizes developing dendrites. Nature. 2002; 418:177–181. [PubMed: 12110889]
21. Oyama F, et al. Gem GTPase and tau: morphological changes induced by gem GTPase in cho cells are antagonized by tau. J Biol Chem. 2004; 279:27272–27277. [PubMed: 15087445]
22. Mahalakshmi RN, et al. Nuclear localization of endogenous RGK proteins and modulation of cell shape remodeling by regulated nuclear transport. Traffic. 2007; 8:1164–1178. [PubMed: 17605760]
23. Finlin BS, et al. Regulation of L-type Ca2+ channel activity and insulin secretion by the Rem2 GTPase. J Biol Chem. 2005; 280:41864–41871. [PubMed: 15728182]
24. Beguin P, et al. Regulation of Ca2+ channel expression at the cell surface by the small G-protein kir/Gem. Nature. 2001; 411:701–706. [PubMed: 11395774]
25. Beguin P, et al. RGK small GTP-binding proteins interact with the nucleotide kinase domain of Ca2+-channel beta-subunits via an uncommon effector binding domain. J Biol Chem. 2007; 282:11509–11520. [PubMed: 17303572]
26. Beguin P, et al. 14-3-3 and calmodulin control subcellular distribution of Kir/Gem and its regulation of cell shape and calcium channel activity. J Cell Sci. 2005; 118:1923–1934. [PubMed: 15860732]
27. Finlin BS, et al. Analysis of the complex between Ca2+ channel beta-subunit and the Rem GTPase. J Biol Chem. 2006; 281:23557–23566. [PubMed: 16790445]
28. Aresta S, de Tand-Heim MF, Beranger F, de Gunzburg J. A novel Rho GTPase-activating-protein interacts with Gem, a member of the Ras superfamily of GTPases. Biochem J. 2002; 367:57–65. [PubMed: 12093360]
29. Ward Y, et al. The GTP binding proteins Gem and Rad are negative regulators of the Rho-Rho kinase pathway. J Cell Biol. 2002; 157:291–302. [PubMed: 11956230]
30. Bader PL, et al. Mouse model of Timothy syndrome recapitulates triad of autistic traits. Proc Natl Acad Sci U S A. 2011; 108:15432–15437. [PubMed: 21878566]

31. Takahashi K, Yamanaka S. Induction of pluripotent stem cells from mouse embryonic and adult fibroblast cultures by defined factors. Cell. 2006; 126:663–676. [PubMed: 16904174]
32. Dolmetsch R, Geschwind DH. The human brain in a dish: the promise of iPSC-derived neurons. Cell. 2011; 145:831–834. [PubMed: 21663789]
33. Yazawa M, et al. Using induced pluripotent stem cells to investigate cardiac phenotypes in Timothy syndrome. Nature. 2011; 471:230–234. [PubMed: 21307850]
34. Pasca SP, et al. Using iPSC-derived neurons to uncover cellular phenotypes associated with Timothy syndrome. Nat Med. 2011; 17:1657–1662. [PubMed: 22120178]
35. Splawski I, et al. Severe arrhythmia disorder caused by cardiac L-type calcium channel mutations. P Natl Acad Sci USA. 2005; 102:8089–8096.
36. Dolmetsch RE, Pajvani U, Fife K, Spotts JM, Greenberg ME. Signaling to the nucleus by an L-type calcium channel-calmodulin complex through the MAP kinase pathway. Science. 2001; 294:333–339. [PubMed: 11598293]
37. Yang J, Ellinor PT, Sather WA, Zhang JF, Tsien RW. Molecular determinants of Ca2+ selectivity and ion permeation in L-type Ca2+ channels. Nature. 1993; 366:158–161. [PubMed: 8232554]
38. Parent L, Gopalakrishnan M. Glutamate substitution in repeat IV alters divalent and monovalent cation permeation in the heart Ca2+ channel. Biophys J. 1995; 69:1801–1813. [PubMed: 8580323]
39. Lee T, Winter C, Marticke SS, Lee A, Luo L. Essential roles of Drosophila RhoA in the regulation of neuroblast proliferation and dendritic but not axonal morphogenesis. Neuron. 2000; 25:307–316. [PubMed: 10719887]
40. Swetman CA, et al. Extension, retraction and contraction in the formation of a dendritic cell dendrite: distinct roles for Rho GTPases. Eur J Immunol. 2002; 32:2074–2083. [PubMed: 12115629]
41. Kranenburg O, et al. Activation of RhoA by lysophosphatidic acid and Galpha12/13 subunits in neuronal cells: induction of neurite retraction. Mol Biol Cell. 1999; 10:1851–1857. [PubMed: 10359601]
42. Totsukawa G, et al. Distinct roles of ROCK (Rho-kinase) and MLCK in spatial regulation of MLC phosphorylation for assembly of stress fibers and focal adhesions in 3T3 fibroblasts. J Cell Biol. 2000; 150:797–806. [PubMed: 10953004]
43. Casanova MF, et al. Minicolumnar abnormalities in autism. Acta Neuropathol. 2006; 112:287–303. [PubMed: 16819561]
44. Belmonte MK, et al. Autism and abnormal development of brain connectivity. J Neurosci. 2004; 24:9228–9231. [PubMed: 15496656]
45. Geschwind DH, Levitt P. Autism spectrum disorders: developmental disconnection syndromes. Curr Opin Neurobiol. 2007; 17:103–111. [PubMed: 17275283]
46. Belmonte MK, Bourgeron T. Fragile X syndrome and autism at the intersection of genetic and neural networks. Nat Neurosci. 2006; 9:1221–1225. [PubMed: 17001341]
47. Kaufmann WE, Moser HW. Dendritic anomalies in disorders associated with mental retardation. Cereb Cortex. 2000; 10:981–991. [PubMed: 11007549]
48. Cohen-Kutner M, Nachmanni D, Atlas D. CaV2.1 (P/Q channel) interaction with synaptic proteins is essential for depolarization-evoked release. Channels (Austin). 2010; 4:266–277. [PubMed: 20495360]
49. Wiser O, et al. The voltage sensitive Lc-type Ca2+ channel is functionally coupled to the exocytotic machinery. Proc Natl Acad Sci U S A. 1999; 96:248–253. [PubMed: 9874804]
50. Tanabe T, Beam KG, Adams BA, Niidome T, Numa S. Regions of the skeletal muscle dihydropyridine receptor critical for excitation-contraction coupling. Nature. 1990; 346:567–569. [PubMed: 2165570]
51. Green EM, Barrett CF, Bultynck G, Shamah SM, Dolmetsch RE. The tumor suppressor eIF3e mediates calcium-dependent internalization of the L-type calcium channel CaV1.2. Neuron. 2007; 55:615–632. [PubMed: 17698014]
52. Gomez-Ospina N, Tsuruta F, Barreto-Chang O, Hu L, Dolmetsch R. The C terminus of the L-type voltage-gated calcium channel Ca(V)1.2 encodes a transcription factor. Cell. 2006; 127:591–606. [PubMed: 17081980]

53. Paradis S, et al. An RNAi-based approach identifies molecules required for glutamatergic and GABAergic synapse development. Neuron. 2007; 53:217–232. [PubMed: 17224404]

54. Xia Z, Dudek H, Miranti CK, Greenberg ME. Calcium influx via the NMDA receptor induces immediate early gene transcription by a MAP kinase/ERK-dependent mechanism. J Neurosci. 1996; 16:5425–5436. [PubMed: 8757255]

55. Kaech S, Banker G. Culturing hippocampal neurons. Nat Protoc. 2006; 1:2406–2415. [PubMed: 17406484]

56. Zhang F, et al. Multimodal fast optical interrogation of neural circuitry. Nature. 2007; 446:633–639. [PubMed: 17410168]

57. Meijering E, et al. Design and validation of a tool for neurite tracing and analysis in fluorescence microscopy images. Cytometry A. 2004; 58:167–176. [PubMed: 15057970]

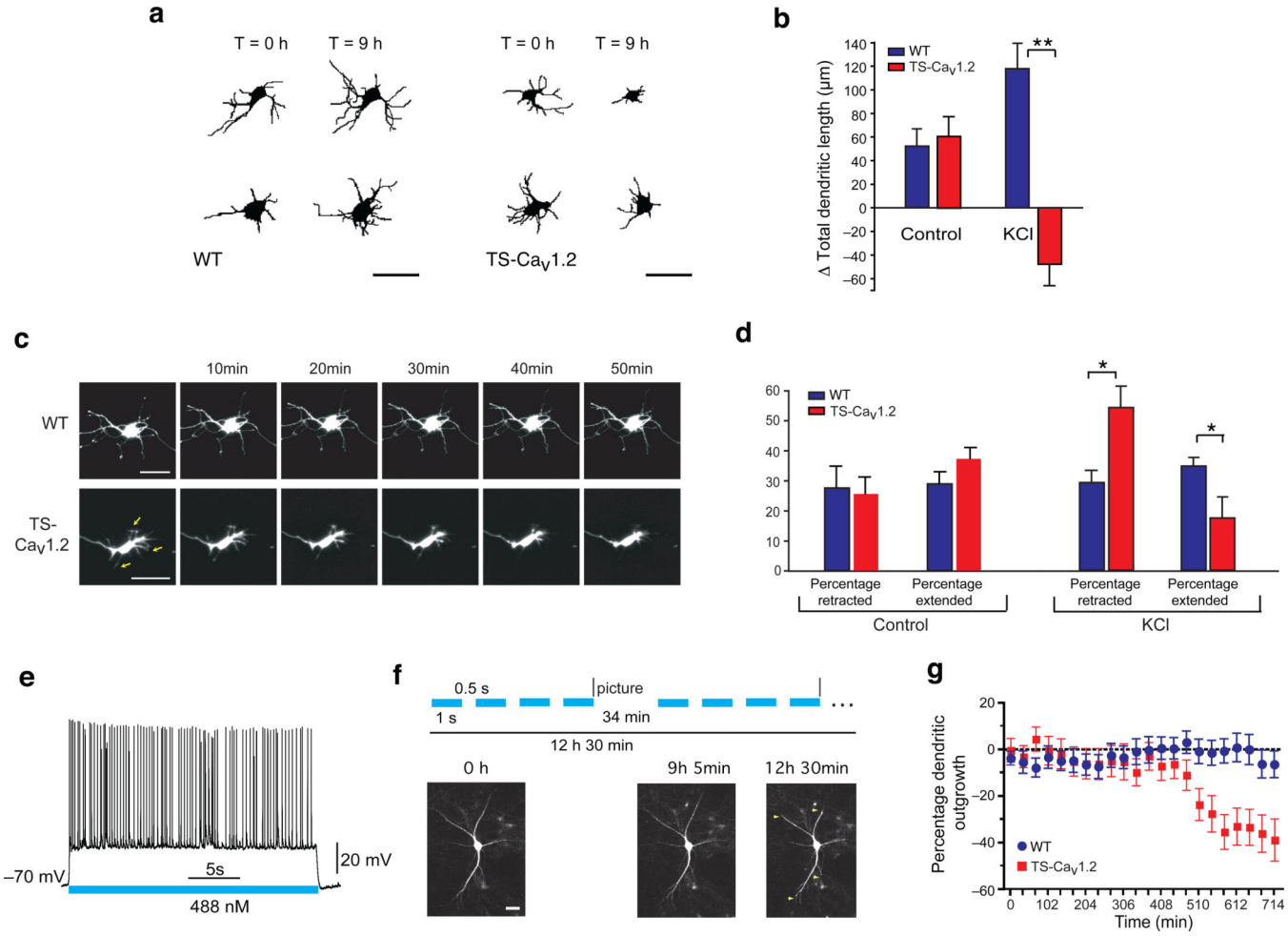

Figure 1. TS- $Ca_V1.2$ causes activity-dependent dendritic retraction

(a) Representative dendrite tracings of dissociated cortical neurons co-transfected with YFP and WT (left) or TS-$Ca_V1.2$ (right) and imaged before and after stimulation with 67 mM KCl. Scale bars are 50 μm. **(b)** Quantification of the change in total dendrite length following KCl stimulation in individual WT or TS-$Ca_V1.2$ transfected neurons (n ≥ 30 cells per condition; mean ± s.e.m.; ** $p<0.001$ by 2-way ANOVA, Bonferroni post-test). **(c)** Epifluorescence images of representative cortical neurons transfected as in (a) and imaged every 10 minutes following depolarization. Neurons transfected with TS-$Ca_V1.2$ show increased retraction of dendrites over the one-hour period (white arrowheads). Scale bar is 50 μm. **(d)** Quantification of the percentage of dendrites that showed an increase (percentage extended) or decrease (percentage retracted) in length of greater than 2 μm after 60 minutes in control or depolarizing (KCl) solutions (n=4 experiments, n≥ 25 dendrites/experiment, mean ± s.e.m., * $p<0.05$ by Student's t-test). **(e)** Representative current clamp recording of a hippocampal neuron expressing channelrhodopsin-2 during illumination with 488 nM light. **(f)** Schematic representing the protocol used for illumination and image acquisition, and epifluorescence images of a representative hippocampal neuron transfected with TS channel. Scale bars are 50 μm. **(g)** Quantification of the percent change in total dendritic outgrowth in

WT (n = 52) or TS-$Ca_V1.2$ (n = 36) expressing neurons over the time course of stimulation (mean ± s.e.m., ** $p<0.001$ by Student's t-test).

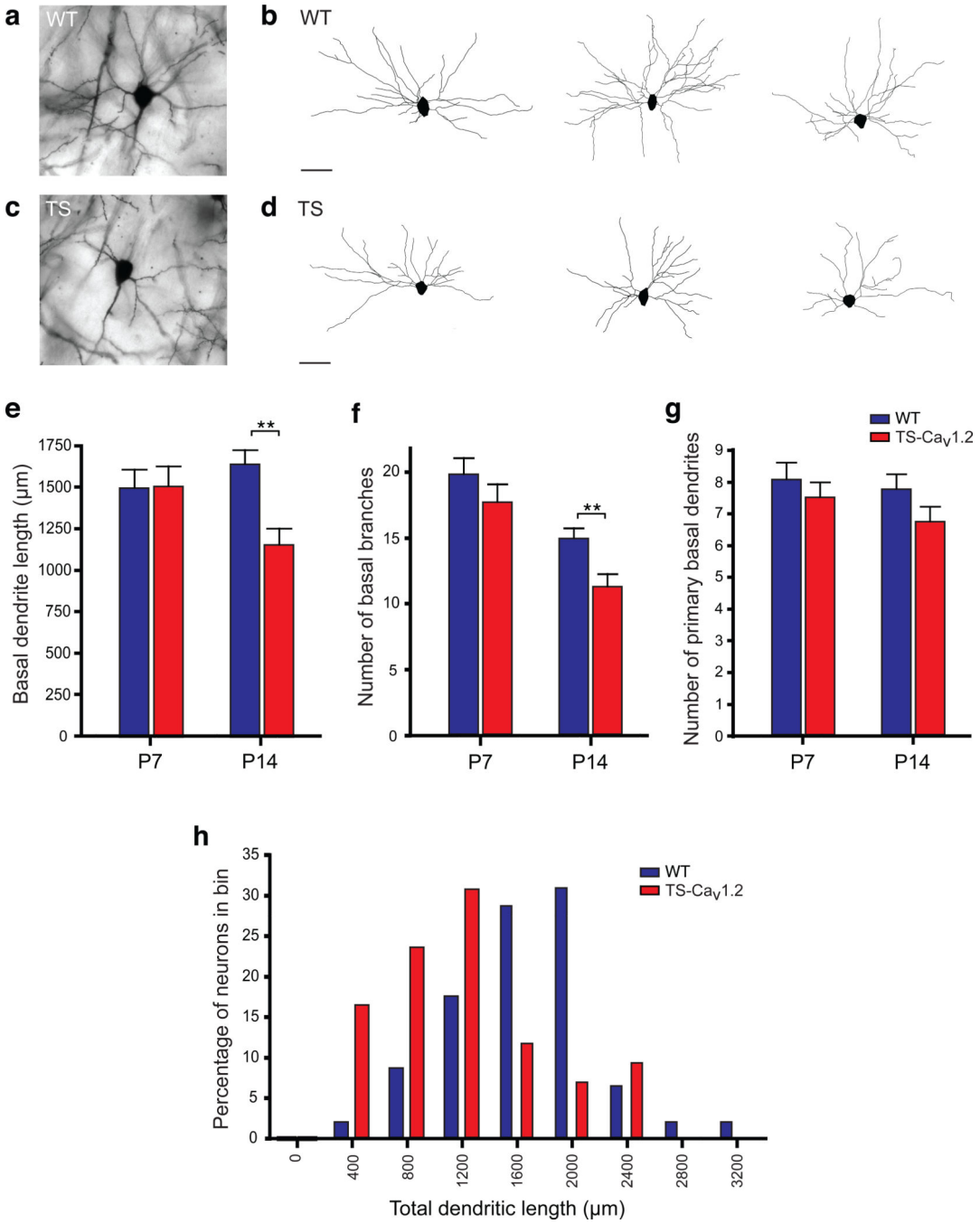

Figure 2. Reduction in dendritic complexity in the basal dendrites of layer 2/3 pyramidal cortical neurons from *TS*+/− mice

(a) and **(c)** Representative images of Golgi-stained layer 2/3 pyramidal neurons from the frontal cortex of WT (a) or $TS^{+/-}$ (c) littermate P14 mice. **(b)** and **(d)** Representative dendrite tracings of the basal dendritic arbors of layer 2/3 pyramidal cortical neurons from WT (b) or $TS^{+/-}$ (d) P14 mice. Scale bars are 100 µm. **(e, f, g)** Average total length of all basal dendrites (e), basal branch number (f) and primary dendrite number (g) of pyramidal neurons from WT or $TS^{+/-}$ mice at P7 (n ≥ 27 neurons from 3 mice of each genotype) or P14

(n ≥ 42 neurons from 5 mice of each genotype). Mean ± s.e.m.; ** p<0.001 by unpaired Student's t-test. **(h)** Histogram of the percentage of neurons from WT (n = 45) or $TS^{+/-}$ (n = 42) mice with different total dendritic lengths. Bin width = 400 μm, numbers on x-axis represent bin center.

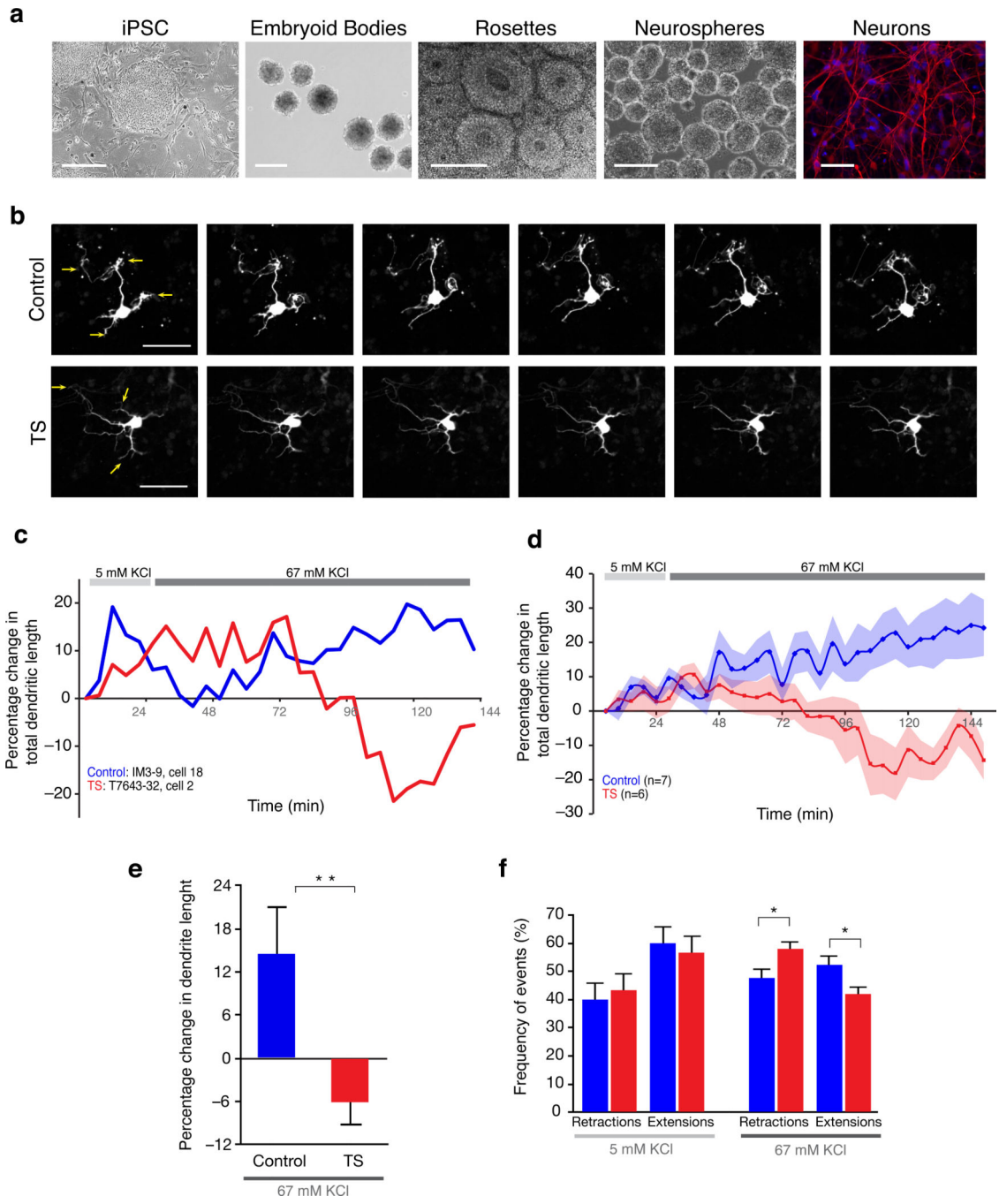

Figure 3. Human iPSCs-derived TS neurons show activity dependent dendritic retraction

(**a**) Panel illustrating the stages of neural differentiation from iPSCs. Representative phase contrast images of iPSC colonies (scale bar 400 μm), embryoid bodies (scale bar 200 μm), neural rosettes (scale bar 200 μm), neurospheres (scale bar 200 μm), and immunocytochemistry of neurons (scale bar 50 μm; MAP2 in red, Hoechst blue). (**b**) Representative time course images of control (upper) and TS (lower) iPSC-derived neurons expressing YFP under the Synapsin-1 promoter. Scale bars are 50 μm. (**c**) Representative dendrite tracings for one control (blue) and one TS (red) neuron before and after stimulation

with 67 mM KCl. (**d**) Average percentage change in total dendritic length over time in control (blue, n= 7 neurons from 2 control lines) and TS (red, n= 6 neurons from one patient line). (**e**) Average percentage change in total dendritic length in control (blue) and TS (red) derived neurons after 120 minutes of incubation in a 67 mM KCl depolarizing solution (n= 27 neurons from 3 control lines derived from 2 subjects, n= 36 neurons from 3 patient lines derived from 2 individuals with TS; **$p < 0.005$ by Student's t-test; mean ± s.e.m.). (**f**) Quantification of the percentage of dendritic retraction (i.e., negative percent change in dendritic length at one particular time point as compared to the previous time point) or extension events (i.e., positive percent change in dendritic length at one particular time point as compared to the previous time point) in control (blue) and TS (red) iPSC-derived neurons in 5 mM KCl solution and in 67 mM KCl depolarizing solution (mean ± s.e.m., * $p<0.05$ by Student's t-test).

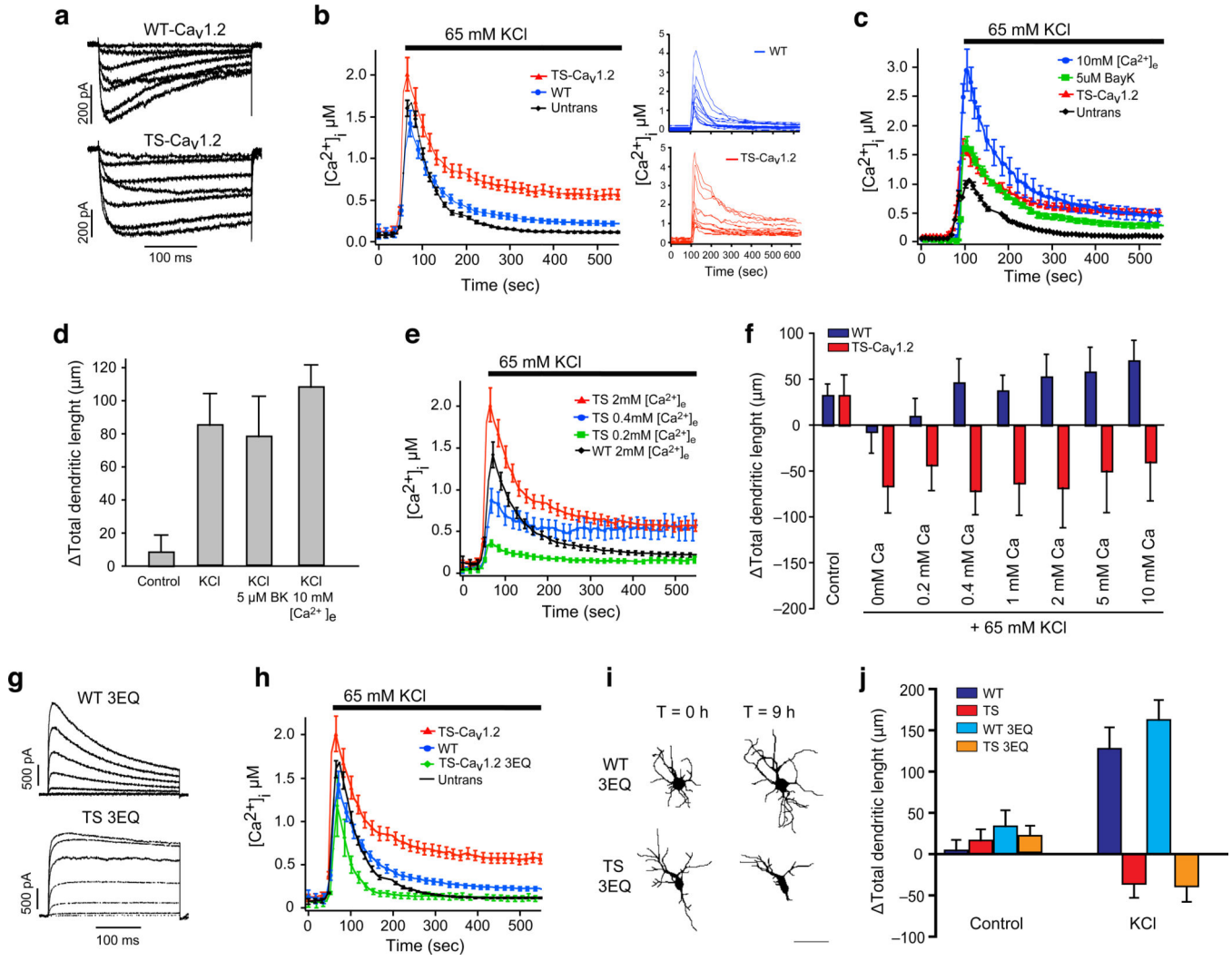

Figure 4. TS-$Ca_V1.2$–mediated dendritic retraction is independent of Ca^{2+} flux through the channel

(a) Representative current traces measured in barium-containing external solution in response to a depolarizing pulse protocol (depicted above) from HEK-293 cells transfected with WT- (top) or TS- $Ca_V1.2$ (bottom) channels. **(b)** Average $[Ca^{2+}]_i$ responses in untransfected dissociated cortical neurons (black) or neurons transfected with WT (blue) or TS (red) channels following depolarization with 67 mM KCl. (n ≥ 45 cells per condition; mean ± s.e.m.). Right hand panels are representative Ca^{2+} traces from individual neurons expressing either WT (blue) or TS-$Ca_V1.2$ (red) channels. **(c)** Average $[Ca^{2+}]_i$ responses in neurons loaded with fura-2 and depolarized in the presence of 5 µM BayK 8644 (green) or 10 mM $[Ca^{2+}]_e$ (blue) as compared to TS-$Ca_V1.2$ transfected cells (red) or untransfected neurons (black) (n ≥ 40 cells; mean ± s.e.m.). **(d)** Quantification of the change in total dendrite length following KCl stimulation in individual cortical neurons depolarized in the presence of 5 µM BayK 8644 (green) or 10 mM $[Ca^{2+}]_e$ as in (a) (n ≥ 20 cells per condition; mean ± s.e.m.). **(e)** Average $[Ca^{2+}]_i$ responses in cortical neurons transfected with TS-$Ca_V1.2$ and depolarized in various $[Ca^{2+}]_e$ as indicated on the graph (n ≥ 30 cells per

condition; mean ± s.e.m.). **(f)** Quantification of the change in total dendrite length in individual neurons transfected with WT or TS-$Ca_V1.2$ and depolarized in various $[Ca^{2+}]_e$ as indicated (n ≥ 20 cells per condition; mean ± s.e.m.). **(g)** Currents measured in response to a depolarizing pulse protocol (depicted above) through WT 3EQ (top) or TS-CaV1.2 3EQ (bottom) channels transiently expressed in HEK-293 cells. No inward currents were detected for either channel. **(h)** Average $[Ca^{2+}]_i$ responses of dissociated cortical neurons transfected with WT-$Ca_V1.2$ (blue), TS-$Ca_V1.2$ (red) or with the pore mutant TS-$Ca_V1.2$ 3EQ (blue) (n ≥ 20 cells per condition; mean ± s.e.m.). **(i)** Representative dendrite tracings of cortical neurons transfected with WT 3EQ or TS-$Ca_V1.2$ 3EQ pore mutant channels and imaged before and after depolarization. Scale bars are 50 μm. **(j)** Quantification of the average change in total dendrite length in individual neurons transfected with WT or TS-$Ca_V1.2$ channels or their 3EQ pore mutant versions (TS = −36.3 ± 16.7 μm; TS 3EQ = −39.3 ± 18.5 μm, n ≥ 50 cells per condition; mean ± s.e.m.).

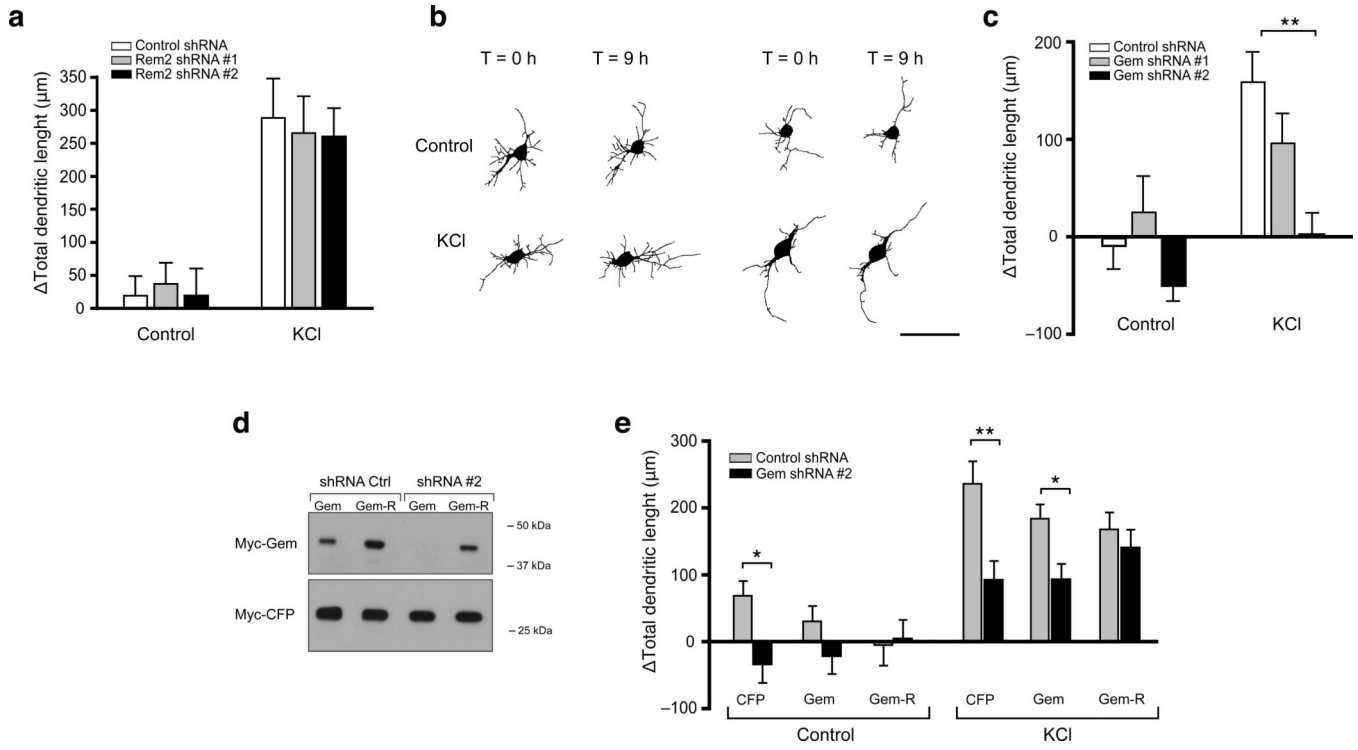

Figure 5. Reducing Gem expression in cortical neurons prevents activity-induced dendritic arborization

(**a**) Quantification of the average change in total dendrite length in dissociated cortical neurons transfected with control shRNA, Rem2 shRNA #1 or Rem2 shRNA #2 after incubation in control or depolarizing conditions (n ≥ 16 cells per condition; mean ± s.e.m.). (**b**) Representative dendrite tracings of cortical neurons transfected with control shRNA or Gem shRNA #2 and imaged before and after depolarization with 67 mM KCl. Scale bars are 50 μm. (**c**) Quantification of the average change in total dendrite length in neurons transfected with control shRNA, Gem shRNA #1 or Gem shRNA #2 in control or depolarizing conditions (n ≥ 20 cells per condition; mean ± s.e.m.; * $p<0.001$ by 2-way ANOVA, Bonferroni post-test). (**d**) Cropped anti-Myc Western blot of lysates from HEK 293T cells co-transfected with Myc-Gem or Myc-Gem-R (which contains silent mutations that render it resistant to Gem shRNA #2) and either control shRNA or Gem shRNA #2. Cells were also transfected with Myc-CFP as a transfection and loading control. Full-length blots are presented in Supplementary Figure 10. (**e**) Quantification of the average change in total dendrite length in neurons co-transfected with control shRNA or Gem shRNA #2 and either CFP, Gem, or the shRNA-resistant Gem-R. The amount of activity-dependent dendritic arborization in neurons transfected with Gem-R and Gem shRNA #2 is not significantly different from that in cells expressing control shRNA (Gem-R + control shRNA = 168.9 ± 23.9; Gem-R + shRNA #2 = 141.6 ± 23.8). (n ≥ 20 cells per condition; mean ± s.e.m.; * $p<0.05$, ** $p<0.001$ by 2-way ANOVA, Bonferroni post-test).

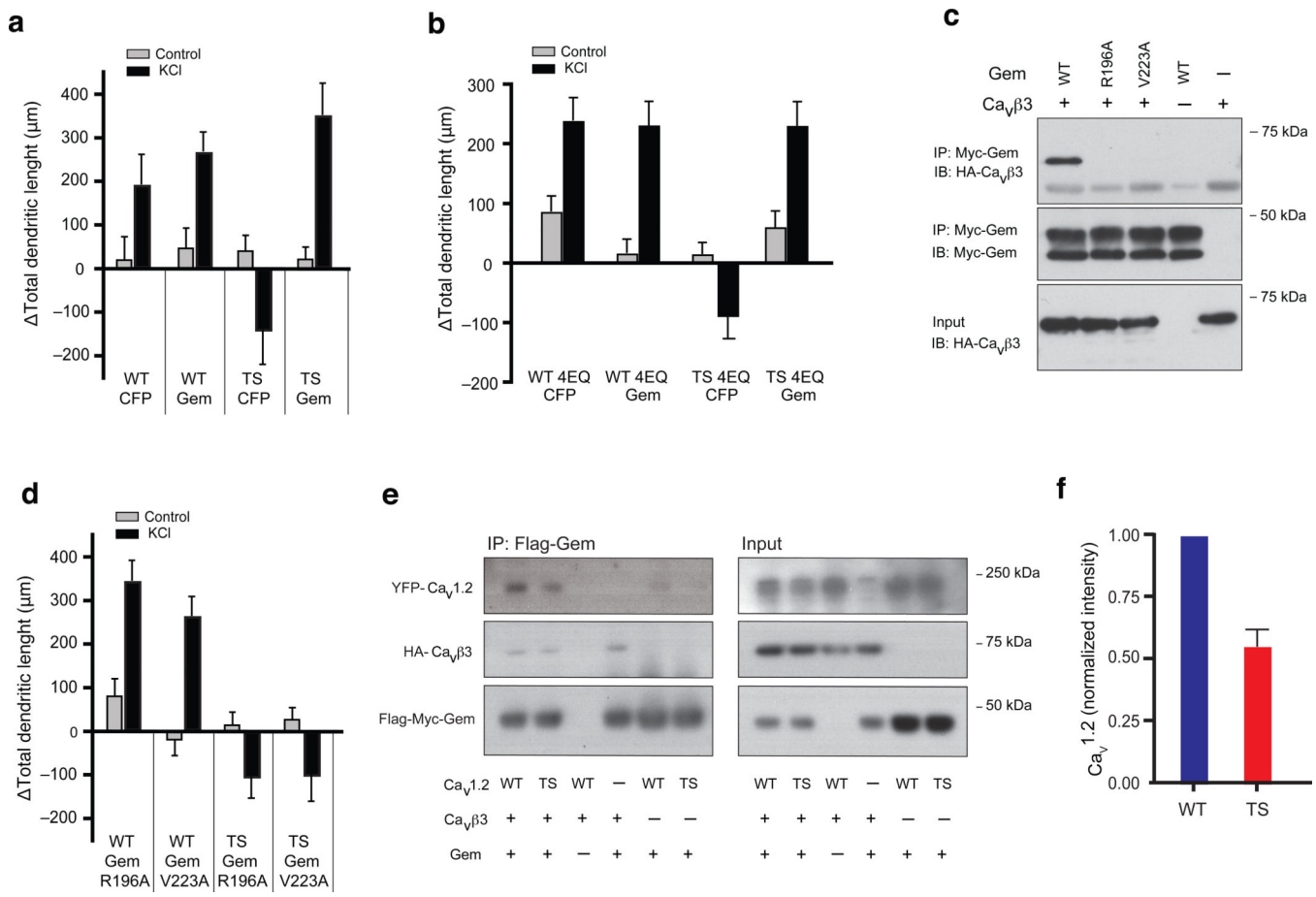

Figure 6. Over-expression of Gem prevents dendritic retraction in TS-Ca$_V$1.2 expressing neurons and its effects are dependent on association with the Ca$_V$β subunit

(**a**) Quantification of the average change in total dendrite length in neurons transfected with WT or TS-Ca$_V$1.2 along with either CFP or Gem (**b**) Quantification of the average change in total dendrite length in neurons expressing CFP or Gem as well as the pore mutant (4EQ) versions of WT or TS-Ca$_V$1.2 channels (n ≥ 17 cells per condition; mean ± s.e.m.). Neurons expressing TS-Ca$_V$1.2 4EQ (TS 4EQ) and Gem show a similar amount of activity-dependent dendritic arborization to neurons expressing WT-Ca$_V$1.2 4EQ channels (TS 4EQ + Gem = 232.2 ± 38.8; WT 4EQ + CFP = 240.9 ± 36.9; WT 4EQ + Gem = 233.1 ± 38.8). (**c**) Immunoprecipitation of HA-Ca$_V$β3 with Myc-Gem in HEK 293T cell lysates. Gem constructs containing point mutations (R196A and V223A), known to prevent association with Ca$_V$β3[25], fail to immunoprecipitate Ca$_V$β3. Full-length blots are presented in Supplementary Figure 10. (**d**) Overexpression of GEM mutants R196A and V223A that do not bind to Ca$_V$1.2 fails to rescue dendritic retraction in TS neurons. **(e)** Immunoprecipitation of YFP-Ca$_V$1.2 and HA-Ca$_V$β3 with Flag-Myc-Gem in lysates of Neuro2a cells that were transfected with either a WT or TS-Ca$_V$1.2 α-subunit as well as HA-Ca$_V$β3 and/or Flag-Myc-Gem. Full-length blots are presented in Supplementary Figure 10. **(f)** Quantification of the relative intensity of co-immunoprecipitated TS-Ca$_V$1.2 channel bands compared to WT channel bands (bars represent average from 3 separate experiments, mean ± s.e.m.).

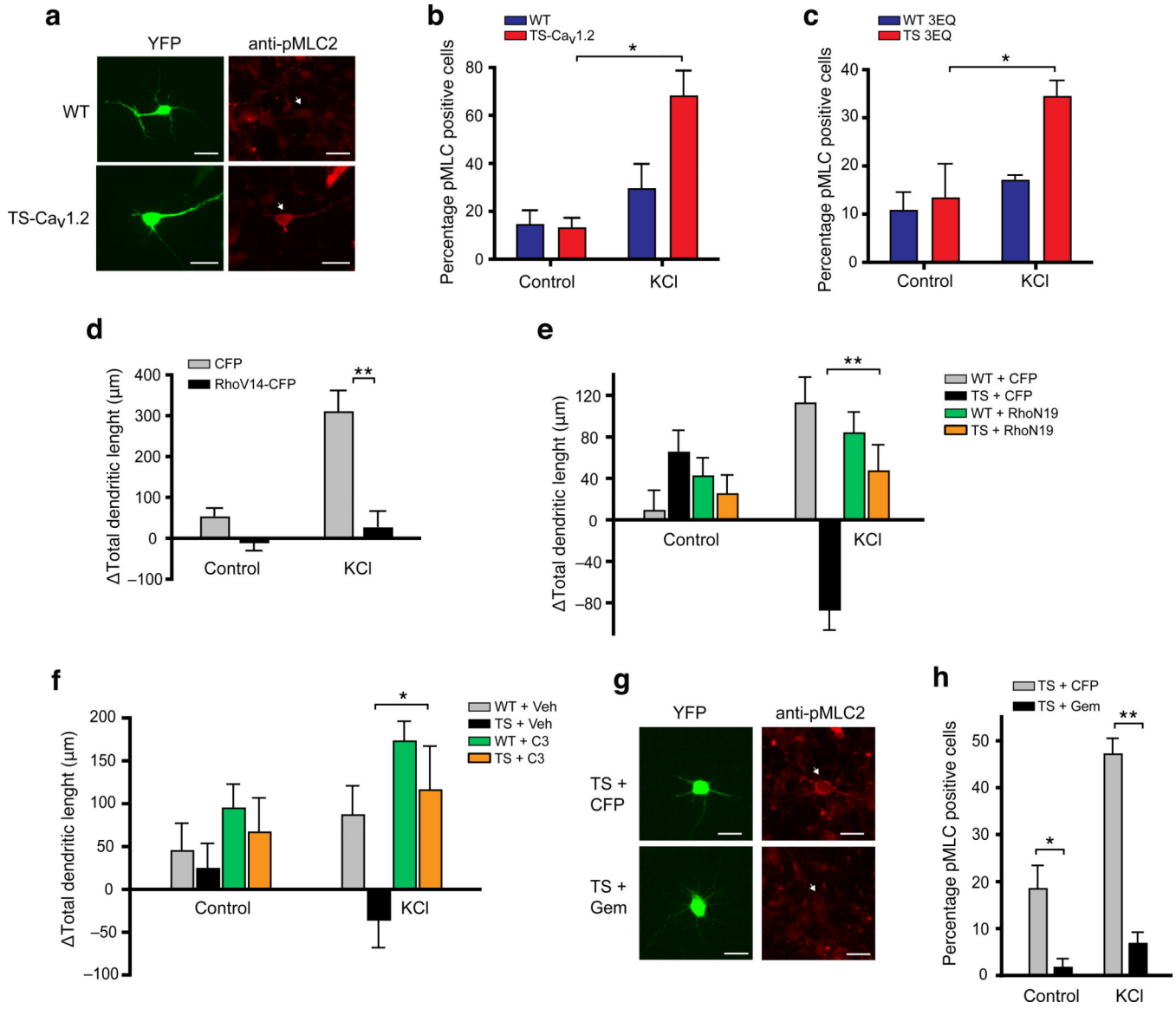

Figure 7. TS-Ca$_V$1.2 causes dendrite retraction by activating RhoA

(**a**) Representative images of YFP (left) and anti-pMLC2 (right) fluorescence in dissociated cortical neurons expressing WT or TS-Ca$_V$1.2 channels after depolarization with 67 mM KCl (white arrows point to transfected cells). Scale bar is 20 μm. (**b**) Quantification of the percent of WT or TS-Ca$_V$1.2 expressing neurons positive for pMLC staining in control or stimulated conditions (bars represent average from 3 separate experiments, n ≥ 40 cells per condition per experiment, mean ± s.e.m., * $p<0.01$ by 2-way ANOVA, Bonferroni post-test). (**c**) Quantification of the percent of WT or TS-3EQ expressing neurons positive for pMLC staining in control or stimulated conditions (bars represent average from 2 separate experiments, n ≥ 40 cells per condition per experiment, mean ± s.e.m., * $p<0.05$ by 2-way ANOVA, Bonferroni posttest). (**d**) Quantification of the average change in total dendrite length in neurons transfected with CFP alone or a CFP-tagged constitutively active RhoA (RhoV14-CFP) following incubation in control or depolarizing (67 mM KCl) solutions (n ≥

15 cells per condition; mean ± s.e.m.; **p<0.001 by 2-way ANOVA, Bonferroni post-test). (**e**) Quantification of the average change in total dendrite length in neurons transfected with WT or TS-$Ca_V1.2$ along with either CFP alone or a CFP-tagged dominant negative RhoA (RhoN19) (n ≥ 20 cells per condition; mean ± s.e.m.; **p<0.001 by 2-way ANOVA, Bonferroni post-test). (**f**) Quantification of the average change in total dendrite length in neurons transfected with WT or TS-$Ca_V1.2$ and depolarized in the presence of 0.5 μg/ml C3 transferase or vehicle alone (n ≥ 15 cells per condition; mean ± s.e.m.; * p<0.01 by 2-way ANOVA, Bonferroni post-test). **(g)** Representative images of YFP (left) and anti-pMLC2 (right) fluorescence in cortical neurons expressing either CFP or Gem and TS-$Ca_V1.2$ channels after depolarization with 67 mM KCl (white arrows point to transfected cells). Scale bar is 20 μm. **(h)** Quantification of the percent of TS-$Ca_V1.2$ expressing neurons positive for pMLC2 staining in control or stimulated conditions (bars represent average from 2 separate experiments, n ≥ 50 cells per condition per experiment, mean ± s.e.m., * p<0.05, ** p<0.001 by 2-way ANOVA, Bonferroni post-test).